



HAL
open science

Is the plateau state in GRS 1915+105 equivalent to canonical hard states?

Pieter van Oers, Sera Markoff, Farid Rahoui, Dipankar Maitra, Michael Nowak, Jörn Wilms, Alberto J. Castro-Tirado, Jerome Rodriguez, Vivek Dhawan, Emilios Harlaftis

► To cite this version:

Pieter van Oers, Sera Markoff, Farid Rahoui, Dipankar Maitra, Michael Nowak, et al.. Is the plateau state in GRS 1915+105 equivalent to canonical hard states?. Monthly Notices of the Royal Astronomical Society, 2010, 409, pp.763-776. 10.1111/j.1365-2966.2010.17339.x . insu-03625619

HAL Id: insu-03625619

<https://insu.hal.science/insu-03625619>

Submitted on 31 Mar 2022

HAL is a multi-disciplinary open access archive for the deposit and dissemination of scientific research documents, whether they are published or not. The documents may come from teaching and research institutions in France or abroad, or from public or private research centers.

L'archive ouverte pluridisciplinaire **HAL**, est destinée au dépôt et à la diffusion de documents scientifiques de niveau recherche, publiés ou non, émanant des établissements d'enseignement et de recherche français ou étrangers, des laboratoires publics ou privés.



Distributed under a Creative Commons Attribution 4.0 International License

Is the plateau state in GRS 1915+105 equivalent to canonical hard states?

Pieter van Oers,¹★† Sera Markoff,¹ Farid Rahoui,^{2,3}‡ Dipankar Maitra,¹§ Michael Nowak,⁴ Jörn Wilms,⁵ Alberto J. Castro-Tirado,⁶ Jerome Rodriguez,² Vivek Dhawan⁷ and Emilios Harlaftis⁸¶

¹*Astronomical Institute ‘Anton Pannekoek’, University of Amsterdam, Science Park 904, 1098 XH, the Netherlands*

²*Laboratoire AIM, CEA/IRFU, Université Paris Diderot, CNRS/INSU, CEA Saclay, DSM/IRFU/Sap, F-91191 Gif sur Yvette, France*

³*AstroParticule & Cosmologie (APC)/Université Paris VII/CNRS/CEA/Observatoire de Paris, Bât. Condorcet, 10 rue Alice Domon et Léonie Duquet, 75205 Paris Cedex 13, France*

⁴*Kavli Institute for Astrophysics and Space Research, Massachusetts Institute of Technology, Cambridge, USA*

⁵*Dr. Karl Remeis-Sternwarte, Astronomisches Institut, Universität Erlangen-Nuremberg, Sternwartstr. 7, 96049, Germany*

⁶*Instituto de Astrofísica de Andalucía (IAA-CSIC), Glorieta de la Astronomía s/n, 18008 Granada, Spain*

⁷*National Radio Astronomy Observatory, 10003 Lopezville Road, Socorro, NM 87801, USA*

⁸*Institute of Space Applications and Remote Sensing, National Observatory of Athens, PO Box 20048, Athens 11810, Greece*

Accepted 2010 July 9. Received 2010 July 8; in original form 2010 February 9

ABSTRACT

GRS 1915+105 is a very peculiar black hole binary that exhibits accretion-related states that are not observed in any other stellar-mass black hole system. One of these states, however – referred to as the plateau state – may be related to the canonical hard state of black hole X-ray binaries. Both the plateau and hard state are associated with steady, relatively lower X-ray emission and flat/inverted radio emission, that is sometimes resolved into compact, self-absorbed jets. However, while generally black hole binaries quench their jets when the luminosity becomes too high, GRS 1915+105 seems to sustain them despite the fact that it accretes at near- or super-Eddington rates. In order to investigate the relationship between the plateau and the hard state, we fit two multiwavelength observations using a steady-state outflow-dominated model, developed for hard-state black hole binaries. The data sets consist of quasi-simultaneous observations in radio, near-infrared and X-ray bands. Interestingly, we find both significant differences between the two plateau states, as well as between the best-fitting model parameters and those representative of the hard state. We discuss our interpretation of these results, and the possible implications for GRS 1915+105’s relationship to canonical black hole candidates.

Key words: accretion, accretion discs – black hole physics – radiation mechanisms: general – galaxies: active – galaxies: jets – X-rays: binaries.

1 INTRODUCTION

The microquasar GRS 1915+105 was discovered on 1992 August 15, by the WATCH all-sky monitor, aboard the Russian GRANAT satellite (Castro-Tirado, Brandt & Lund 1992; Castro-Tirado et al. 1994). It is a hard X-ray transient located in the constellation of

Aquila, at $l = 45.37^\circ$, $b = -0.22^\circ$, and was the first stellar mass accreting black hole binary (BHB) discovered to exhibit superluminal velocities in its radio emitting-ejecta (Mirabel & Rodriguez 1994). The obvious parallels to the jets in active galactic nuclei (AGN) led to this source being classified as a ‘microquasar’ (Mirabel & Rodríguez 1998). Subsequent observations with instruments on board the *Rossi X-ray Timing Explorer (RXTE)* have revealed a richness in variability, distinguishing GRS 1915+105 from every other known BHB, over which astronomers are still puzzling to this day.

The longer-term X-ray variability exhibits ‘dipping’ that is thought to be associated with the recession and regeneration of the inner parts of the accretion disc, perhaps caused by the onset of thermal–viscous instabilities (Belloni et al. 1997a,b). Other models have interpreted the spectral changes as resulting from the disappearance of the corona (Chaty 1998; Rodriguez et al. 2008a,b), or

*E-mail: pvo1g09@soton.ac.uk

†Present address: School of Physics & Astronomy, University of Southampton, Highfield, Southampton SO17 1BJ.

‡Present address: Harvard University, Department of Astronomy & Harvard Smithsonian Center for Astrophysics, 60 Garden Street, Cambridge, MA 02138, USA.

§Present address: Department of Astronomy, University of Michigan, 500 Church St., Ann Arbor, MI 48109, USA.

¶In Memoriam.

from the dissipation of magnetic energy via magnetohydrodynamical plasma processes (e.g. Tagger et al. 2004).

Beyond the dipping behaviour, Belloni et al. (2000) were able to classify all variability patterns stretching over more than a year into only 12 classes (Klein-Wolt et al. 2002; Hannikainen et al. 2005 later identified two more classes), based on colour–colour diagrams and light curves. Ten of these 12 classes can be understood as the interplay of two or three of three basic states, designated as states A, B and C. The remaining two classes, ϕ and χ , do not show state transitions and appear exclusively within states A and C, respectively. State A displays the highest flux and the softest spectrum while state C displays the lowest flux and the hardest spectrum. Although state B never lasts for more than a few hundred seconds, ϕ and χ episodes can persist for days or short intervals of <100 s.

Aside from the existence of so many distinct accretion states, GRS 1915+105 appears similar to other BHBs. Thus there has been much discussion (e.g. Reig, Belloni & van der Klis 2003) about the extent to which any of the states found in GRS 1915+105 correspond to the ‘canonical’ states (see, e.g. Homan & Belloni 2005; Remillard & McClintock 2006 for definitions) found in the average BHB. BHBs generally spend the majority of their time in the hard state (HS), which is associated with a low accretion rate, a hard X-ray power-law component with photon index $1.4 \leq \Gamma \leq 2.1$ and steady radio emission with an optically thick, flat-to-inverted spectrum. Sources that persist in the HS for several weeks generally show clear correlations between the radio and X-ray luminosities ($L_R \propto L_X^{0.7}$) (Corbel 2000; Corbel et al. 2003; Gallo, Fender & Pooley 2003). More recently, evidence for a similar correlation between the near-infrared (NIR) and X-ray bands has also been found (Russell et al. 2006; Coriat et al. 2009). Similar to the other BHBs, GRS 1915+105 also displays periods of relatively hard, steady X-ray emission, but in contrast to the HS, only for about half the observation time (Trudolyubov 2001). Belloni et al. (2000) identify these intervals of decreased variability with long C-state episodes. The subset of state C/class χ observations that are radio-bright are referred to as the *plateau* state (Belloni et al. 2000), but elsewhere have variously been referred to as the radio-loud, radio-plateau or radio loud low/hard X-ray state (Muno et al. 2001), the type II hard steady state (Trudolyubov 2001) and χ_{RL} (Naik & Rao 2000).

The plateau state was first described by Foster et al. (1996) and its description was later refined in Fender et al. (1999). The state can assert itself in a period as short as a day and is characterized by a decrease in X-ray flux density and an increase in radio flux density to a steady value, typically ~ 10 – 100 mJy. Ample evidence supports the fact that the plateau state X-ray and radio luminosities are indeed correlated, with an increasing delay from X-ray to infrared (IR) to radio emission (e.g. Klein-Wolt et al. 2002). As in the HS the plateau radio spectrum is optically thick, and au-scale self-absorbed compact jets have been spatially resolved using very long baseline interferometry (VLBI) (Dhawan, Mirabel & Rodríguez 2000; Fuchs et al. 2003b). Another marker of the plateau state comes from timing analyses, where 1–10 Hz quasi-periodic oscillations (QPOs) are present (Rao et al. 2000). The exact frequency of these QPOs appears to be inversely correlated with the radio and soft X-ray flux (Rodríguez et al. 2002; Rau & Greiner 2003).

In line with these arguments, it is tempting to identify the plateau state as GRS 1915+105’s analog of the HS. However, although the plateau state shares many similarities with HS, it does display some distinct properties that cannot be ignored. For instance, while the BHBs in the HS usually have a luminosity of $\lesssim 10$ per cent L_{Edd} , the

average luminosity observed in the plateau state is $\sim L_{\text{Edd}}$. Moreover, the plateau X-ray photon index is never very hard, with $\Gamma \sim 1.8$ – 2.5 (Fender & Belloni 2004). Finally, Reig et al. (2003) argue that the canonical HS is never seen in GRS 1915+105 because a power-law tail (with no exponential cut off) is always present in the plateau state hard X-rays. Although the origin of such tails in the softer states of canonical BHBs is still under debate, it is generally not associated with the HS.

In this work, we seek to make a more quantitative comparison between the plateau state found in GRS 1915+105 and the HS found in more typical black holes, in the context of an outflow-dominated model that has successfully described broad-band data from several BHBs. In Section 2 we describe the multiwavelength data and the reduction methods. We discuss what physical parameters we use for modelling and why in Section 3 and the model itself, together with the results in Section 4. We put our work into context with the findings of others in Section 5, before drawing our final conclusions in Section 6.

2 OBSERVATIONS AND DATA REDUCTION

Based on the light curves and its position in the hardness intensity diagram (HID) diagram (see Figs 1–3), GRS 1915+105 was in a class χ state on 1999 July 8 (data set 1) and 2005 April 13 (data set 2). The presence of a 2–5 Hz QPO on both occasions (see Fig. 4) corroborates this fact. During the 1999 episode, quasi-simultaneous radio and near-infrared observations were performed using the United Kingdom Infra-Red Telescope (UKIRT) and the Green Bank Interferometer (GBI). The 2005 data set also holds observations of the Cerro Tololo Inter-American Observatory (CTIO) and Ryle telescope. Details on the observations and reduction methods are found in the individual sections and Table 1. The 2005 *RXTE* data are also extensively analysed and discussed in Rodríguez et al. (2008a,b).

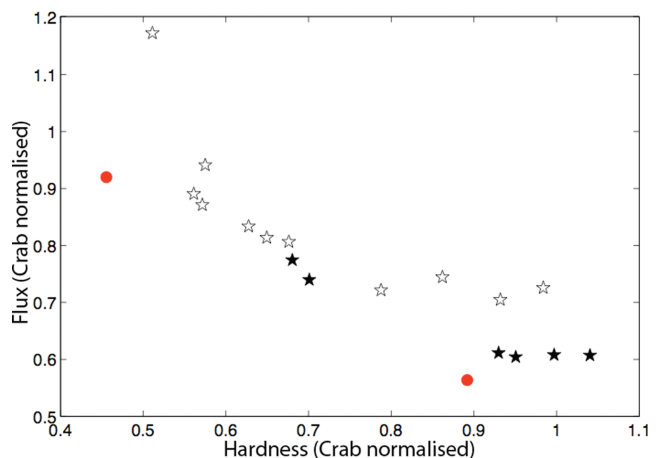


Figure 1. HID comparing our observations (filled circles) to the plateau states from Belloni et al. (2000) (data courtesy of T. Belloni; open stars are $\chi 1$, closed stars are $\chi 3$). The soft, higher-luminosity red dot is ObsID 90105-07-02-00, the lower is ObsID 40403-01-09-00. The plot shows the hardness and flux, normalized to Crab units, calculated by taking the ratio and the sum of the *RXTE* PCU 2 rates in two bands: channel 0–35 (~ 2 – 15 keV) and 36–49 (~ 16 – 21 keV). Each band is divided by the Crab rate in the same band, on the same day, simulating a photon index of 2.1 and utilizing a normalization of $10 \text{ photons cm}^{-2} \text{ s}^{-1} \text{ keV}^{-1}$ at 1 keV.

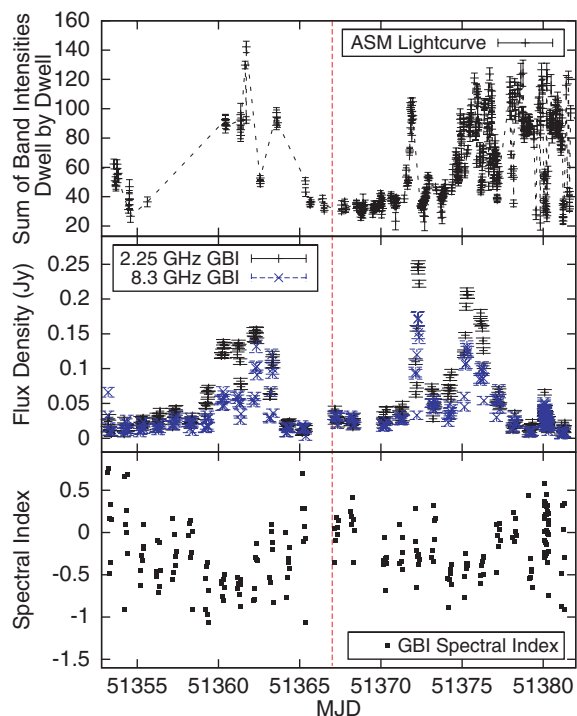


Figure 2. GRS 1915+105 X-ray, NIR and radio light curves for the 1999 data set. Also, the radio spectral index, as measured by the Green Bank Interferometer is shown. The red dashed line indicates the time of the *RXTE* observation.

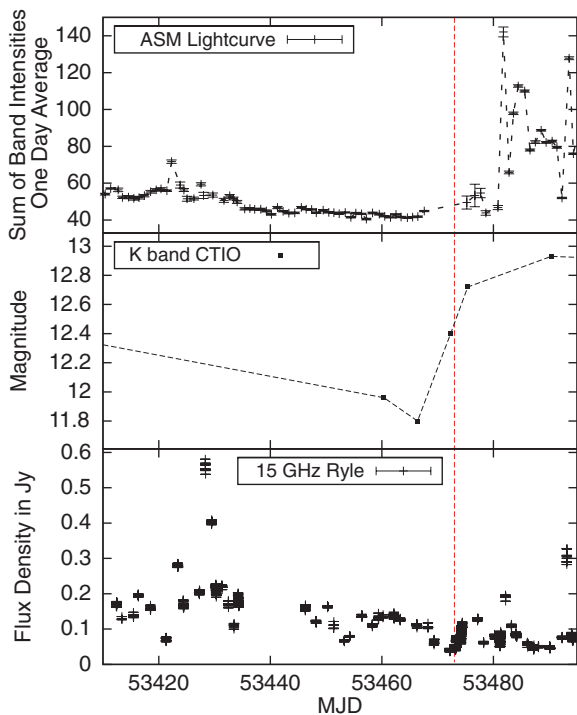


Figure 3. GRS 1915+105 X-ray and radio light curves for the 2005 data set. The radio light curve was measured by the Ryle Telescope (Pooley & Fender 1997). The red dashed line indicates the time of the *RXTE* observation.

2.1 X-ray: *RXTE* data reduction

We use data from two instruments on board the *RXTE*: the Proportional Counter Array (PCA; Jahoda et al. 2006) and the High En-

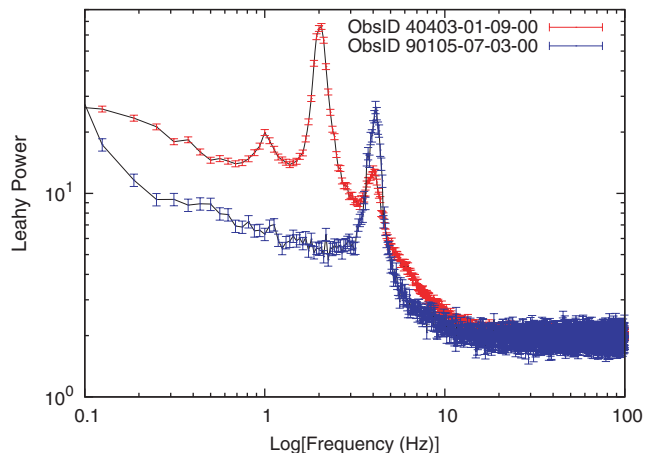


Figure 4. Normalized (following Leahy et al. 1983) power density spectra showing the type-C QPOs in the X-rays for both data sets, indicating the observations are plateau state. (Courtesy of P. Soleri).

ergy X-ray Timing Experiment (HEXTE; Rothschild et al. 1998). The X-ray data have been reduced using *HEASOFT*, version 6.3.1., applying standard extraction criteria: a pointing offset of $<0.01^\circ$ from the nominal source position, and a source elevation of $>10^\circ$. The exclusion time for the South Atlantic anomaly (SAA), however, was only 10 min, as GRS 1915+105 is a very bright source. For the same reason we disregarded the top layer and imposed a maximum ‘electron ratio’ of 2, to take into account contamination by source photons. All HEXTE data products were dead-time corrected. Correction for the PCA dead-time was also carried out; proportional counter unit (PCU) 4 was inactive for half of the 1999 observation, while during the other half, both PCU 1 and 4 were inactive. The 2005 observation was done with PCU 0 and 2 only. Due to uncertainties in the first four PCA channels, we only include PCA data above 3 keV. The PCA calibration falls off rapidly above ~ 25 keV and since HEXTE provides reliable data for energies $\gtrsim 20$ keV we ignored the PCA data above 22 keV. For the PCA, standard2f mode data were used. The PCA background was modelled using the *pca_bkgd_cmbrigtvle_eMv20051128* model. Only HEXTE data above 20 keV were used due to the uncertainty of the response matrix below these energies. At high energies, the spectrum was ignored above 200 keV. We rebinned the X-ray data to a minimum S/N of 4.5.

2.2 NIR: UKIRT data reduction and CTIO

On 1999 July 08, medium-resolution spectroscopic observations of GRS 1915+105 were performed with the Cooled Grating Spectrometer (CGS4) mounted on the UKIRT (PI Harlaftis). 24 spectra in the B1 and 18 in the B2 filters were acquired, each time at two nodding positions, giving a total exposure time of 1260 s in B1 and 1080 s in B2. Moreover, the telluric standard HD 176232, a F0p main sequence star, was observed in the same conditions.

All the spectra were reduced with *IRAF* through bad pixel correction, flat fielding and sky subtraction. The target spectra were then extracted and wavelength calibrated by extracting, in the same condition, krypton and argon spectra in B1 and B2, respectively. They were combined and telluric feature-corrected through the division by the standard star spectrum. We finally multiplied the corrected spectrum by a F0V star one from the ISAAC synthetic spectra

Table 1. Observations included in data set 1 and 2, with *RXTE* ObsID 40403-01-09-00 and 90105-07-02-00, respectively. The *H* and *K* bands, obtained using the Cooled Grating Spectrometer on UKIRT, are at 1.455–2.094 and 1.906–2.547 μm , respectively (*J* band measurements were also done, but these are unusable due to high interstellar extinction). The *K*-band observation in data set 2 was done (more than half a day before ObsID 90105-07-02-00) with the ANDICAM at CTIO. The GBI measurements are 2.25 and 8.3 GHz and the flux densities used are 30-s vector scan averages. The Ryle telescope operates at 15 GHz and the flux density used is the average of ~ 13 ks worth of 5-min integrations.

Data set 1 1999 July 8/MJD 51367					Data set 2 2005 April 13/MJD 53473				
Band	Instrument	MJD start	UTC	Duration	Instrument	MJD start	Time	Duration	
X-ray	<i>RXTE</i>	51367.2737	06:34:13	14 435 s	<i>RXTE</i>	53473.054	01:09:05	6769 s	
NIR	UKIRT	(<i>H</i>)	51367.4821	11:34:10	80 min	CTIO (<i>K</i>)	53472.3216	07:43:06	25 min
		(<i>K</i>)	51367.8216	07:56:59	64 min				
Radio	GBI	51367.371	09:02:53	30 s	Ryle	53473.098	02:21:07	219 min	

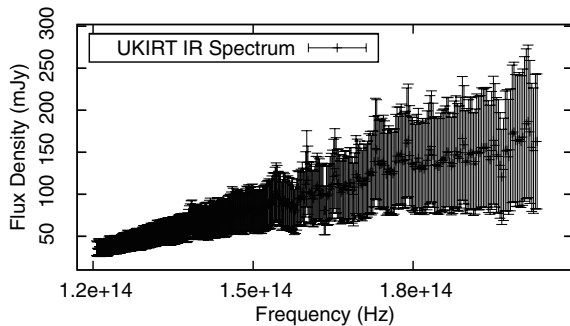


Figure 5. NIR spectrum of the 1999 data set.

library,¹ resampled to the CGS4 resolution and flux-scaled to match the HD 176232 magnitudes in *H* and *Ks*. The uncertainty of the flux calibration obtained this way is about 5 per cent.

The spectra were then dereddened using the extinction laws given in (Cardelli, Clayton & Mathis 1989) and (Chiar & Tielens 2006), assuming a hydrogen column density of $N_{\text{H}} = 3.5 \times 10^{22} \text{ cm}^{-2}$, i.e. $A_{\text{V}} = 19.6 \pm 1.7$ (Chapuis & Corbel 2004). The errors resulting from using the two different methods were then added in quadrature. The overall propagated uncertainties, combining flux calibration and dereddening, represent about 20 per cent of the flux. The final spectrum is shown in Fig. 5.

The UKIRT spectrum included in data set 1 was also rebinned, because the spectral resolution is well beyond what we need for continuum fitting (see Section 4).

The 12.40-mag *K*-band point in data set 2 was taken using the CTIO 1.3-m telescope using the ANDICAM (A Novel Double-Imaging CAMera) detector (Neil, Bailyn & Cobb 2007). It was dereddened using the same method as the UKIRT data. However, we chose the error bars to account for the fact that GRS 1915+105 may have been approaching a state transition: The source magnitude varies from 11.8 to 12.72 in about 9 d (see Fig. 3), suggesting a dereddened flux density of 67.85 ± 27.25 mJy. On MJD 53473 we also see the flux in radio increasing (see below).

2.3 Radio: GBI and Ryle Telescope

Data set 1 includes two GBI data points and data set 2 includes a data point from Ryle Telescope. Light curves from these telescopes are shown in Figs 2 and 3, respectively.

For the GBI data, a flux density calibration procedure similar to that reported in Waltman et al. (1994) has been employed here. The flux densities of 0237 – 233, 1245 – 197 and 1328 + 254 were determined using observations of 1328 + 307 (3C 286). The flux density of 3C 286 was based on the scale of Baars et al. (1977), and the assumed values were 11.85 Jy at 2.25 GHz and 5.27 Jy at 8.3 GHz.² On MJD 51367.371 the GBI flux densities were 25 ± 4 mJy at 2.25 GHz and 30 ± 6 mJy at 8.3 GHz. Similar behaviour was shown during a plateau state of 2000 April (Ueda et al. 2002).

The Ryle Telescope operates at 15 GHz and it observed GRS 1915+105 (simultaneously with ObsID 90105-07-02-00) from MJD 53473.098 to MJD 53473.417. The data used here are from Rodriguez et al. (2008a) and were reduced following Pooley & Fender (1997); observations of Stokes I+Q were interwoven with those of a nearby phase calibrator (B1920+154). The flux-density scale was set by reference to 3C48 and 3C286, and should be consistent with that defined by Baars et al. (1977).

On MJD 53473 we see the average radio flux density increasing from 44.9 ± 3.0 to 70.4 ± 4.3 mJy (Rodriguez et al. 2008b), in addition to the IR light curve also suggesting that in spite of the HID classification, GRS 1915+105 may not have strictly been in a plateau state. For this data set we therefore use the average from MJD 53473.098 to 53473.25 of 44.9 ± 3 mJy, closest to the *RXTE* and CTIO observations.

3 CONSTRAINTS ON INPUT PHYSICAL PARAMETERS

In order to meaningfully compare broad-band spectra, we will fit our data sets using a model designed for simultaneous radio through X-ray data sets. Historically, the modelling of BHBs has focused on accretion flow models of only the X-ray emission, of which Comptonizing corona models have been particularly successful. However, in recent years, the evidence is mounting that the bipolar jet outflows found in the HS contribute significantly across the broad-band continuum. For bright transients, e.g. Russell et al. (2006, 2010) estimate up to 90 per cent of the NIR and up to 100 per cent in the X-rays could be dominated by jet production. Other observations of radio/IR/X-ray correlations (Corbel et al. 2000, 2003; Coriat et al. 2009) can be interpreted by either synchrotron or synchrotron-self Compton (SSC) processes relating to the jets. The outflow-dominated model of Markoff, Nowak & Wilms (2005) (hereafter: MNW05) is still the only model that

¹ <http://www.eso.org/sci/facilities/paranal/instruments/isaac/tools/lib/index.html>

² <http://www.gb.nrao.edu/fgdocs/gbi/plgbi/README>

Table 2. Fixed physical parameters used in the fitting process, obtained from the literature. We omit the error bars, as they are not used in the fits.

Parameter	Value	Units	Reference
Column density	4.7	10^{22} cm^{-2}	a
Mass	14 and 23	M_{\odot}	b
Inclination	66 and 50	$^{\circ}$	c
Distance	11 and 6	kpc	c, d
Donor temperature	4455	K	e

References: a, Chaty et al. (1996); b, Greiner et al. (2001a); c, Fender et al. (1999); d, Chapuis & Corbel (2004); e, Alonso et al. (1999).

can fit the X-ray spectrum with the same precision as the coronal models (MNW05; Nowak et al., in preparation) while also fitting the radio through IR bands from the same physical picture. The MNW05 model has already been applied successfully to many Galactic sources in the ‘canonical’ HS: the original paper features fits to Cyg X-1 and GX 339-4, while a different data set of the latter, along with observations of XTE J1118+480 are fit in Maitra et al. (2009). Further papers have explored applications to simultaneous broad-band data sets from GRO J1655-40 and A0620-00 (Gallo et al. 2007; Migliari et al. 2007), with other sources in progress. The result of all these applications has been the discovery, perhaps not surprisingly, that the free parameters fit into similar ranges for all stellar mass sources.

Furthermore, the discovery of a Fundamental Plane of black hole accretion (Merloni, Heinz & di Matteo 2003; Falcke, K rding & Markoff 2004) supports mass-scaling accretion physics from stellar to supermassive BHs, and thus would argue that the MNW05 should also apply to weakly accreting AGN. Confirming this, Markoff et al. (2008) successfully fit several spectral energy distributions (SEDs) from the supermassive BH M81* with parameters in the ranges found from BHBs.

There exists, therefore, a solid framework for the modelling of BHBs in the canonical HS, against which to test fits of data from the GRS 1915+105 plateau state. In this paper we do not consider whether MNW05 is correct but rather use it as a benchmark to test how far GRS 1915+105 fits the phenomenology of the hard state.

Whenever possible, we fixed values for model physical parameters in accordance with those found in other publications during the fitting process. In the following subsections, we first discuss how we obtained these values (presented in Table 2), and then briefly summarize the MNW05 model and our fitting methods before presenting our results.

3.1 Distance and hydrogen column density

The distance to GRS 1915+105 is still a matter of some debate. A first estimate was derived in Mirabel & Rodr guez (1994). From a core ejection they find a maximum distance of 13.7 kpc, under the assumption that the ejection was intrinsically symmetric. Rodr guez et al. (1995) attempted to derive a more accurate distance estimate by determining the kinematic distance from 21-cm absorption spectra of atomic hydrogen along the line of sight to GRS 1915+105 during a radio outburst, and find that it could be as far away as 12.5 ± 1.5 kpc. Later measurements of the $^{12}\text{CO}(J = 1 - 0)$ spectrum by Chaty et al. (1996) are consistent with this distance. They also constrain the visual extinction to be $A_v = 26.5 \pm 1.7$ mag, corresponding to a total hydrogen column density of $N_{\text{H}} = 4.7 \pm 0.2 \times 10^{22} \text{ cm}^{-2}$.

If GRS 1915+105 resides at 12.5 kpc, it must be accreting above the Eddington limit ($L_{\text{X-ray}} \sim 2.9 \times 10^{39} \text{ erg s}^{-1}$; McClintock & Remillard 2003, giving $L_{\text{X-ray}}/L_{\text{Edd}} \sim 1.5$, using a mass of $14 M_{\odot}$; see the next section). A slightly lower maximum distance of 11.2 ± 0.8 kpc, derived from proper motion studies of radio ejecta during four major events (Fender et al. 1999), would still give a ratio $L_{\text{X-ray}}/L_{\text{Edd}} \sim 1.3$.

However, this distance could be too large. Chapuis & Corbel (2004) measure $^{12}\text{CO}(J = 1 - 0)$ velocity spectra of clouds along the line of sight, as well as of two nearby HII regions, and re-evaluate the hydrogen column density to $N_{\text{H}} = 3.5 \pm 0.3 \times 10^{22} \text{ cm}^{-2}$. This column gives a visual extinction of $A_v = 19.6 \pm 1.7$ mag, reducing the number intervening molecular clouds, and arguing for a smaller distance to GRS 1915+105 of 9.0 ± 3.0 kpc (at 9 kpc the accretion rate estimate drops below Eddington), based on evidence that GRS 1915+105 lies behind the molecular hydrogen cloud G 45.45+0.06. This cloud is at ~ 7 kpc (Feldt et al. 1998); however, Chapuis & Corbel (2004) suggest that this cloud belongs to a huge complex, located at a distance of 6 kpc, providing the above lower limit to the distance (the upper limit of 12 kpc is from Fender et al. 1999). However, the high column density required (Mirabel & Rodr guez 1994; Rodr guez et al. 1995) suggests that another molecular cloud should be between us, therefore Fender et al. (1999) adopted the conservative distance of 11 kpc.

Considering the assumptions made in Chapuis & Corbel (2004) and the resulting size of the error bars, we have decided to follow Fender et al. (1999) in adopting a more conservative distance of 11 kpc for this work. This distance is consistent with $N_{\text{H}} = 3.5 \pm 0.3 \times 10^{22} \text{ cm}^{-2}$, which we believe is the correct value pertaining to the IR band, as well as the larger hydrogen column density of $4.7 \times 10^{22} \text{ cm}^{-2}$ from Chaty et al. (1996), that we use for our X-ray fits, motivated by the works of, e.g. Klein-Wolt et al. (2002) (see Section 5).

Because a distance of 11 kpc implies super-Eddington luminosities for GRS 1915+105, we also fit the data using the minimum distance of 6 kpc, in order to explore the importance of distance on the modelling conclusions.

3.2 GRS 1915+105 black hole mass

In order to constrain the mass of the compact object in a binary via the mass function, the orbital period, inclination and the mass of the companion (or the mass ratio) must all be known. Greiner, Cuby & McCaughrean (2001a) found an orbital period P_{orb} of 33.5 d and a velocity amplitude $K = 140 \pm 15 \text{ km s}^{-1}$, giving a mass function $f(M) = 9.5 \pm 3.0 M_{\odot}$. Assuming that the binary plane is the same as that of the accretion disc, the orbital inclination can be estimated from the orientation of the jets. As no constant precession has been observed, the jets can be assumed to be perpendicular to the accretion disc and orbital plane. The exact inclination is however still open to debate, as it is determined from the brightness and velocities of both the approaching and receding blobs. At a distance of 11 kpc the inclination is $i = 66^{\circ} \pm 2^{\circ}$ (Fender et al. 1999). Harlaftis & Greiner (2004) were able to deduce a mass ratio $M_d/M_x = 0.053 \pm 0.033$ from the rotational broadening of photospheric absorption lines of the donor star. Together these values give a mass for GRS 1915+105 of $14.0 \pm 4.4 M_{\odot}$ (Greiner et al. 2001a). We use these as our fiducial values for the distance and mass. For the 6 kpc distance, we calculate a smaller inclination of $i = 50^{\circ}$ using Fender et al. (1999), and, using Harlaftis & Greiner (2004) a mass of $23 M_{\odot}$.

3.3 Properties of the donor star

A rough identification of the companion was performed by Greiner et al. (2001b), by analysing absorption line features in the NIR. They conclude that the companion is a class III K-M giant and compare it successfully to a K2 III star. If the star is indeed a K2 III giant, its temperature should be $T_d = 4455 \pm 190$ K (Alonso, Arribas & Martínez-Roger 1999), and accretion proceeds via Roche-lobe overflow (Greiner et al. 2001b). We use this temperature for the simplistic blackbody spectral component representing the companion in our spectral fits.

4 MODELLING AND RESULTS

4.1 Description of model

For all spectral fits we use the program *ISIS* (Houck & Denicola 2000) compiled with XSPEC version 12.3.1x libraries (Arnaud 1996). The model discussed below is forward-folded through the X-ray detector response matrices, but applied directly to the radio through NIR data. To account for the additional uncertainties in the PCA response matrix, a 0.5 per cent systematic error has been added in quadrature to all PCA data. As the relative calibration of the PCA and HXTE instruments is not certain, the normalization factor for the PCA data is set to unity and tied to the radio and NIR normalizations during the fits, while the HEXTE data normalization is left free to vary.

As the focus of our paper is on modelling the non-thermal spectrum, and the exact stellar model needed for GRS 1915+105 is uncertain, we use a simple blackbody to model the NIR, with the temperature fixed as discussed in the previous section. This component serves to account for the excess IR/optical flux level due to the star, so that the overall model normalization is correct.

In addition to the jet and the star we have an outer accretion flow in the form of a ‘standard’ geometrically thin accretion disc (Shakura & Sunyaev 1973). This flow is parametrized by the radius of the inner and outer disc edges (r_{in} , r_{out}) and the temperature at the inner edge (T_{in}). In the Schwarzschild geometry, the innermost stable circular orbit has a radius of $6 r_g$, but this radius can be reduced to $1 r_g$ in the Kerr metric, when the BH is maximally spinning. The disc component serves to both fit spectral signatures of thermal emission from the accretion flow in the X-ray band, as well as contributing seed photons for inverse Compton scattering, but is only a weak element in comparison to the entire spectrum.

We now summarize the physical parameters in our jet (see Table 3). One of the most important of these parameters is the jet luminosity (N_j). This factor scales with the accretion power at the inner edge of the accretion disc and represents the power going into the jet and acts as a normalization factor. The power is equally divided to supply the internal and kinetic pressures. We assume that the kinetic energy is carried by cold protons, while the leptons do the radiating. The energy involved in the internal pressure goes into the particle and magnetic energy densities, with a ratio determined by k , where $k = 1$ equals equipartition and higher values indicate magnetic dominance. The initial velocity at the base of the jet, or ‘nozzle’, is the proper sound speed of an electron/proton plasma: $\beta\gamma c \sim 0.4c$. The radius of the jet-base is also a free parameter, r_0 (expressed in units of gravitational radius $r_g = GM/c^2$). The particles start off in a quasi-thermal (relativistic) Maxwellian distribution, the peak energy of which is determined by the electron temperature (T_e). Beyond the nozzle the jet is allowed to expand freely, or adiabatically, causing a longitudinal pressure gradient. This pressure gradient leads to a moderate acceleration of the jet along the

direction of flow; the resulting velocity profile is calculated from the Euler equations and is roughly logarithmic, evening out at bulk speeds with Lorentz factors of $\Gamma \sim 2-3$ (see, e.g. Falcke, Markoff & Bower 2009). In a segment of the jet located at some variable distance (z_{acc} ; also expressed in r_g) from the base, we assume a significant fraction (75 per cent) of the leptons is accelerated into a power law. The slope of the power-law particle distribution p is also not pre-determined. In each jet segment after the acceleration front, the general shape of the distribution is assumed to remain the same, while the total lepton density decreases according to the adiabatic expansion. This is achieved assuming a continuous injection of ‘fresh’ energetic power-law distributed electrons ($N(E)dE \propto E^{-p}dE$) in each segment after the acceleration region. The jet is stopped at a distance z_{max} from the base.

All fits are done using the following components: (1) The MNW05 steady-state outflow-dominated model that includes a multicolour blackbody accretion disc and a single blackbody for the companion star; (2) an additive Gaussian line profile, with a line energy left free to vary between 6 and 7 keV, and line width σ free to vary between 0 and 2 keV; Models (1)+(2) are either convolved with Compton reflection from a neutral medium (reflect; Magdziarz & Zdziarski 1995) or multiplied with the smeared edge model (smedge; Ebisawa 1991; using the ‘standard’ index for the photoelectric cross-section of ~ -2.67), that accounts for relativistic smearing of the iron line, and multiplied with a photoelectric absorption model (phabs) to account for the interstellar medium. As the strength of an absorption feature (or edge) is related to the strength of the according emission line, the line width is in principle also related to the absorption edge width. Thus when using the smedge model, we tie the width of the edge to the width of the Gaussian. For the reflect model we assume the viewing angle to correspond to the jet inclination. Furthermore, although the reflect model already includes an absorption edge, it is a sharp unsmeared edge, therefore we also tried fitting the data with both the smedge and reflect models.

4.2 Spectral fitting and results

The results of all fits are presented in Figures 6–11, with respective parameters listed in Table 3. Below we discuss the individual fits to both data sets in more detail.

Initial fits revealed that, in the case of GRS 1915+105, using smedge is statistically preferred to using reflect, to model the reflection features above ~ 10 keV. Therefore, we proceed to fit the data in greater detail with the smedge model, but include a fit that employs reflect as this model has been used generally to model the disc reflection in previous works (see Section 3).

The spectral index of the optically thick radio-NIR synchrotron emission is determined in part by the internal jet plasma parameters such as the electron temperature, but it is most sensitive to the Doppler beaming factor (calculated from the inclination of the jets). The closer the jet axis aligns with the line of sight, the less inverse the observed radio spectrum. Fixing the inclination according to observation and choosing a jet length for all fits of 10^{16} cm, sufficient so that the slope through the radio data points is continuous, reveals a key difference between the two GRS 1915+105 plateau state data sets and canonical BHs. In order to avoid too much excess in the NIR over the companion star BB, and to provide the best NIR fit, the initial particle acceleration region in the jets z_{acc} needs to be at a distance of at least $\sim 10^4 r_g$. Therefore, the post-acceleration region in the jets does not dominate the X-ray emission below ~ 10 keV, in

Table 3. Parameter ranges found in canonical black holes GX339-4 (Markoff et al. 2005; Maitra, Markoff & Brocksopp 2009), XTE J1118+480 (Maitra et al. 2009), Cyg X-1 (Markoff et al. 2005), GRO J1655-40 (Migliari et al. 2007) and A0620-00 (Gallo et al. 2007), during the HS and best-fitting parameters for the GRS 1915+105 plateau state. The error bars have been resolved at 90 per cent confidence level. We failed to resolve the error bars for parameters listed in italics. N_j is the jet normalization; r_0 is the nozzle radius; T_e is the temperature of the leptons as they enter the jet; p is the spectral index of the radiating particles; k is the ratio between magnetic and electron energy densities; z_{acc} is the location of the particle acceleration region in the jet; $f_{\text{scat}} = 0.36/$ is the ratio between scattering mean free path and gyroradius; L_{disc} and T_{disc} are the luminosity and temperature of the accretion disc; A_{HXT} is the relative normalization between HEXTE and PCA; A_{line} , E_{line} and σ are the normalization, the energy and width of the iron line feature; E_{edge} and τ_{max} are the energy and the normalization of the smedge model iron line edge (the iron edge width is the same as that of the Gaussian); and $\Omega/2\pi$ is the reflection fraction from the reflect model.

Variable	Units	GRS 1915+105						
		Range found in canonical BHBs	MJD 51367			MJD 53473		
			SMEDGE	REFLECT	SMEDGE2	6KPC	ELTEMP	SYNCH
N_j	$10^{-1} L_{\text{Edd}}$	0.0034–0.71	$4.78^{+0.01}_{-0.00}$	$6.45^{+0.00}_{-0.01}$	$9.91^{+0.01}_{-0.00}$	$2.22^{+0.01}_{-0.01}$	$13.65^{+0.00}_{-0.41}$	<i>1.99</i>
r_0	GM/c^2	3.5–20.2	$20.39^{+0.01}_{-0.01}$	$9.30^{+0.01}_{-0.00}$	$6.45^{+0.00}_{-0.00}$	$4.94^{+0.05}_{-0.01}$	$4.18^{+0.24}_{-0.15}$	$3.6^{+0.6}_{-0.6}$
T_e	10^9 K	20–52.3	$9.21^{+0.00}_{-0.01}$	$7.70^{+0.01}_{-0.00}$	$8.45^{+0.00}_{-0.00}$	$9.01^{+0.06}_{-0.01}$	$3.94^{+0.00}_{-0.02}$	8.38
p		2.1–2.9	$2.30^{+0.05}_{-0.06}$	$2.10^{+0.03}_{-0.05}$	$1.84^{+0.01}_{-0.00}$	$2.53^{+0.06}_{-0.04}$	$2.14^{+0.08}_{-0.03}$	$1.16^{+0.03}_{-0.03}$
k		1.1–7	692^{+1}_{-1}	270^{+1}_{-1}	$28.9^{+0}_{-0.1}$	95^{+2}_{-3}	707^{+68}_{-265}	200
z_{acc}	$10^3 GM/c^2$	0.007–0.4	<i>844</i>	<i>30</i>	20^{+4}_{-1}	<i>7.4</i>	<i>9</i>	<i>17</i>
ϵ_{sc}	10^{-4}	1.6–299	<i>0.48</i>	<i>0.91</i>	$0.87^{+0.02}_{-0.03}$	<i>1.7</i>	<i>0.75</i>	$0.90^{+0.22}_{-0.19}$
r_{in}	GM/c^2	0.1–486	$2.54^{+0.00}_{-0.06}$	$2.91^{+0.02}_{-0.02}$	$4.67^{+0.04}_{-0.06}$	$0.62^{+0.00}_{-0.01}$	$4.32^{+0.53}_{-0.54}$	$3.6^{+0.5}_{-0.5}$
L_{disc}^b	$10^{-1} L_{\text{Edd}}$	0.007–0.99	0.91	1.26	1.51	0.73	2.49	1.82
T_{disc}	keV	0.06–1.53	$0.86^{+0.00}_{-0.01}$	$0.83^{+0.00}_{-0.00}$	$0.68^{+0.01}_{-0.00}$	$0.88^{+0.02}_{-0.05}$	$0.81^{+0.03}_{-0.04}$	$0.82^{+0.04}_{-0.06}$
A_{HXT}		-	$0.91^{+0.01}_{-0.01}$	$0.91^{+0.00}_{-0.01}$	$0.92^{+0.00}_{-0.01}$	$0.91^{+0.01}_{-0.01}$	$0.90^{+0.01}_{-0.01}$	$0.90^{+0.02}_{-0.01}$
A_{line}	10^{-3}	-	37^{+5}_{-2}	80^{+3}_{-2}	48^{+2}_{-2}	29^{+2}_{-2}	28^{+8}_{-4}	25^{+6}_{-3}
E_{line}	keV	-	$6.31^{+0.10}_{-0.05}$	$\dagger 6.00^{+0.06}_{-0.00}$	$\dagger 6.00^{+0.04}_{-0.00}$	$6.34^{+0.09}_{-0.12}$	$6.35^{+0.09}_{-0.09}$	$6.36^{+0.09}_{-0.09}$
σ	keV	-	$0.81^{+0.10}_{-0.06}$	$1.32^{+0.05}_{-0.05}$	$0.92^{+0.06}_{-0.07}$	$0.67^{+0.17}_{-0.14}$	<i>0.22</i>	<i>0.07</i>
$\Omega/2\pi$		0.00–0.35	-	$\dagger 0.30^{+0.00}_{-0.01}$	-	-	-	-
E_{edge}	keV	-	$9.15^{+0.15}_{-0.11}$	-	$8.87^{+0.14}_{-0.13}$	$9.08^{+0.18}_{-0.16}$	$9.09^{+0.25}_{-0.16}$	$9.13^{+0.22}_{-0.25}$
τ_{max}	10^{-2}	-	12^{+1}_{-2}	-	19^{+1}_{-1}	12^{+1}_{-2}	11^{+2}_{-2}	10^{+1}_{-2}
χ^2/DoF			113/147 (=0.77)	150/148 (=1.02)	166/147 (=1.13)	131/147 (=0.89)	59/81 (=0.73)	59/81 (=0.73)

MNW05 Canonical Parameter Ranges and GRS 1915+105 Best-Fitting Parameters

\dagger Value is pushing lower or upper boundary and is therefore not well constrained.

^b Derived from model values for r_{in} and T_{disc} .

contrast to canonical BHBs in the hard state where acceleration is found to begin on the order of 10s of r_g .

In general we obtain values for electron energy index $p \sim 2.2$ that result in a significant synchrotron contribution to the X-rays below ~ 20 –50 keV, with a ratio of synchrotron to inverse Compton flux of ~ 0.1 . The steeply declining X-ray flux above ~ 20 keV is best fitted by a dominant inverse Compton contribution from the base of the jets. With a much harder value of p we could conceivably fit more of the X-ray emission via synchrotron emission, but only if the exponential decay shape plays a significant role (see Fig. 11 for such a fit to data set 2). For very soft values of the spectral index, synchrotron emission will not contribute significantly, but fits without any synchrotron contribution to the X-ray at all are not statistically favoured.

The exact spectral shape and normalization in the post-acceleration synchrotron component (fitting the radio data) are very dependent on the value of p . When calculating a local statistical minimum, the fitting routine naturally favours the plethora of X-ray data points over the few radio data points, in finding the confidence limits for p , explaining non-negligible systemic residuals in the radio.

For clarity we note that below we will use SMALL CAPS to refer to fits and will continue to use the roman font to refer to models.

4.2.1 Data set 1

The best-fitting models for data set 1 are shown in Figs 6–9 (corresponding to Table 3, SMEDGE, REFLECT, SMEDGE2 and 6KPC column, respectively; see below for explanation of these fit names). The fits are in general statistically good, with a large contribution to the residuals coming from the inadequacy of a simple blackbody to fit the NIR data (see Fig. 5). Completely removing the NIR data from the best-fitting SMEDGE models is an improvement in the $\Delta\chi_{\text{red}}^2$ of ~ 0.08 , to $\chi_{\text{red}}^2 = 0.69$.

Our best-fitting SMEDGE, employing the smedge model also shows the most extreme behaviour in terms of the distribution of the energy budget (evident from the value for the magnetic dominance k) and the acceleration front distance z_{acc} . In addition, this fit is likely to suffer from pair production (see Table 4 and Section 5). Hence we explore several fits with less extreme physical properties, including two more fits employing a smedge model, (SMEDGE2 and

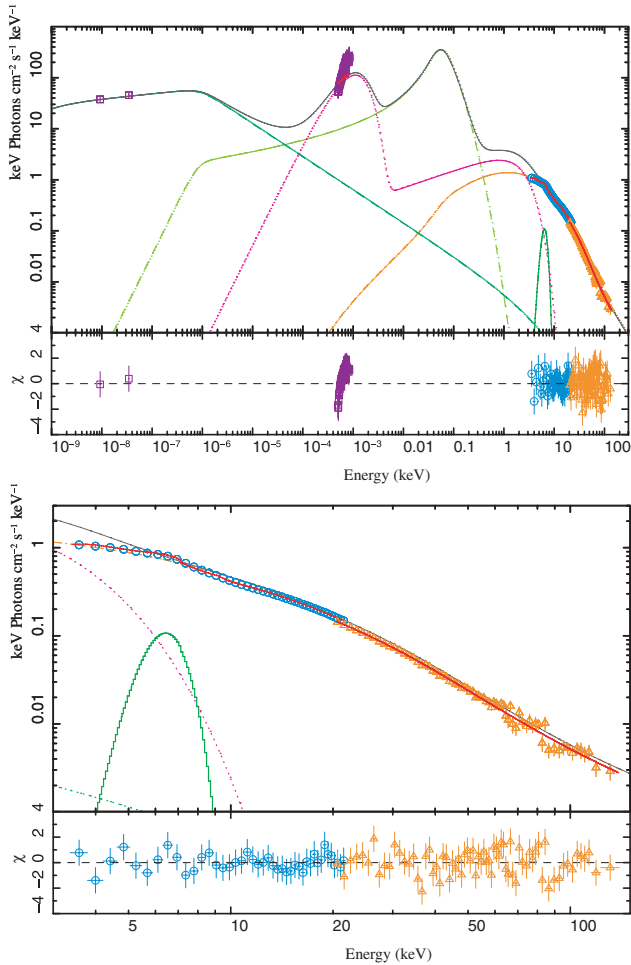


Figure 6. Multiwavelength (top) and X-ray band only (bottom) best-fitting ($\chi^2_{\text{red}} \sim 1.16$) model spectrum (cf. Table 3, SMEDGE column), using MNW05+Gaussian+smedge. Individual contributions from the MNW05 model are also shown: The light-green dashed curve is the pre-shock synchrotron contribution. The dark-green dash-dotted curve is the post-shock synchrotron. The purple dotted curve represents the thermal contributions from the stellar blackbody (below $\sim 10^{-2}$ keV) and the accretion disc. The orange dashed-dotted line above $\sim 10^{-3}$ keV represent the Compton-upscattered stellar blackbody and accretion disc seed photons and the Synchrotron Self-Comptonization (SSC) of the pre-shock synchrotron. The solid grey line is the total MNW05 model spectrum originating from the jet, the accretion disc and the companion; however, it is not forward-folded through the detector response matrices and without iron line or reflection contributions or absorption due to the interstellar hydrogen column density or the smedge model. The red solid lines through the data points show the model flux including all these features. The iron line complex, modelled by a Gaussian, is shown by the thick green curve near 6.4 keV.

6KPC) and one fit using the reflect model (REFLECT). The SMEDGE and SMEDGE2 fits are different local minima that primarily differ from each other in the distribution of the energy budget, most importantly the latter fit has a reduced value for the magnetic dominance k and particle distribution index p . For 6KPC we reduced the distance to GRS 1915+105 to 6 kpc (see below). These fits clearly show over an order of magnitude decrease in z_{acc} and a factor of 2–25 reduction in k . Moreover, pair production will be less important. We note here that fixing z_{acc} to $2 \times 10^4 r_g$ in the SMEDGE fit results in only a minor increase in χ^2_{red} of 0.05, while producing virtually the same model parameters. This suggests that in this case our model does not con-

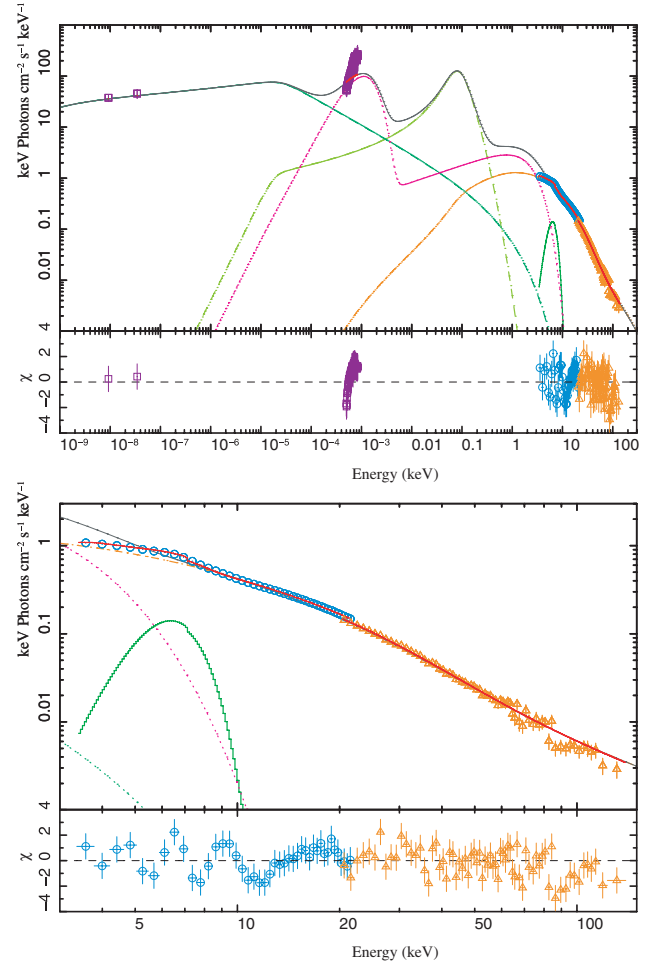


Figure 7. Multiwavelength (top) and X-ray band only (bottom) best-fitting ($\chi^2_{\text{red}} \sim 1.48$) model spectrum (cf. Table 3, REFLECT column), using MNW05+Gaussian+reflect.

verge and shows artefacts from the fitting routine that tries to find the absolute local minimum (within the tolerance limit), although there is no real physical basis for this insignificant improvement. Hence for the SMEDGE fit we will ignore the value for z_{acc} but include the other parameter values in our analysis.

The steeper optically thin synchrotron spectrum of SMEDGE2 could be reconciled with the steeper p found in canonical BHBs by assuming that both share such a hard injected power law, and considering the effect of cooling on the spectrum. We do not consider cooling explicitly here, but are investigating such issues in a separate work. Because of the diminishing magnetic field strength along the jets, the cooling (dominated by synchrotron losses) is negligible. The break energy where the particle distribution steepens in ‘particle space’ shifts according to $E \propto B^{-2} \propto r^2$ (Kardashev 1962). Thus the further along the jet we go, the less important cooling becomes, and thus the largest contribution to the higher frequencies from synchrotron radiation is from the first acceleration zone. Because this zone occurs almost 2 orders of magnitude further out in GRS 1915+105 compared to BHBs, this effect could explain why we are seeing the uncooled injected spectrum rather than the cooled spectrum, expected to be steeper by 0.5.

From the arguments outlined in the previous section it is clear that the true distance to GRS 1915+105 could be much smaller than the 11 kpc adopted for most of our fits. In an attempt to explore

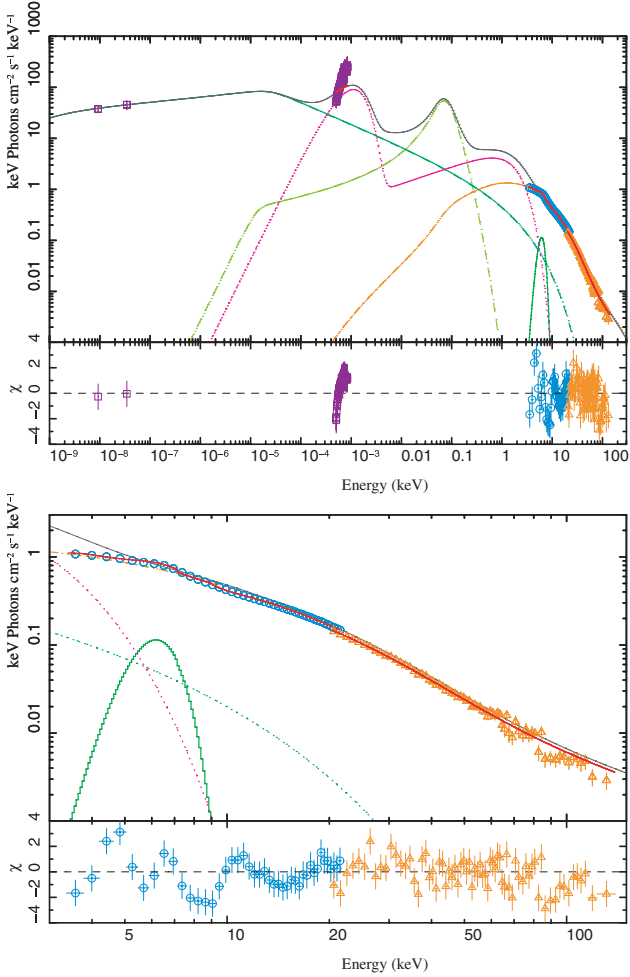


Figure 8. Multiwavelength (top) and X-ray band only (bottom) best-fitting ($\chi^2_{\text{red}} \sim 1.44$) model spectrum (cf. Table 3, SMEDGE2 column), also employing MNW05+Gaussian+smedge, but with a reduced magnetic dominance ($k \sim 30$ in stead of ~ 550 , see Table 3).

the effect of distance, we performed one fit on data set 1 with the distance to GRS 1915+105 reduced to 6 kpc (see Fig. 9 and Table 3, 6kpc column). The modifications result in a similar χ^2_{red} but some values are closer to what we have come to expect for the HS in other black holes. First we find z_{acc} to be the smallest of all fits. This can be understood from the smaller inclination of 50° corresponding to the smaller distance, resulting in a less inverse radio spectrum and hence a lower flux level at the IR break. In addition, the jet luminosity N_j and the partition parameter k are closer to values found for other BHs. With $N_j \sim 0.22L_{\text{Edd}}$ and $k \sim 90$, they are only a fraction of the values found for most 11 kpc fits. Also, the smaller nozzle radius $r_0 \sim 5$ is more typical of the usual HS value. One possible interpretation of these results is that GRS 1915+105 might in fact be closer than the conservative value usually given in the more recent literature.

4.2.2 Data set 2

The best-fitting models for data set 2 are shown in Figs 10 and 11 (corresponding to Table 3, column, ELTEMP and SYNCH, respectively). ELTEMP offers the best comparison – in terms of what component fits what feature – to data set 1, and owes its name to its low electron

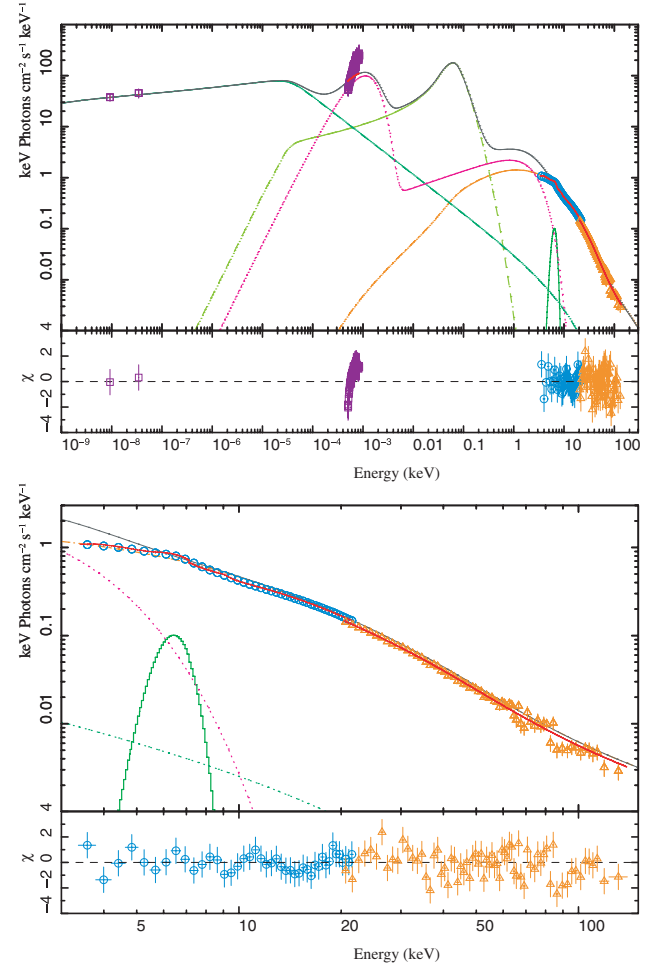


Figure 9. Multiwavelength (top) and X-ray band only (bottom) best-fitting result ($\chi^2_{\text{red}} \sim 1.01$) spectrum (cf. Table 3, 6kpc column), for the 1999 data set, using MNW05+Gaussian+smedge and employing a fixed distance of 6 kpc.

Table 4. Relative importance of pair production processes at the base of the jet, for the statistically good fits in Table 3. n is the lepton number density per cm^{-3} , \dot{n}_{pa} and \dot{n}_{pp} are the pair annihilation rate and production rate per $\text{cm}^{-3} \text{s}^{-1}$, respectively. In order to compare the production rates to the lepton density, they have been multiplied by an estimate for the *residence time*, given by r_0/c . If $n \gg \text{Max}(\dot{n}_{\text{pa}}, \dot{n}_{\text{pp}})$, and $\dot{n}_{\text{pa}} > \dot{n}_{\text{pp}}$ we should be safe from pair production. From these two considerations, the former is the most important.

Fit	r_0 in r_g	$\log(n)$	$\log(\dot{n}_{\text{pa}} \times r_0/c)$	$\log(\dot{n}_{\text{pp}} \times r_0/c)$
SMEDGE	20	15.3	12.9	15.0
REFLECT	9.3	16.1	14.3	15.7
SMEDGE2	6.4	16.6	15.1	15.8
6KPC	4.9	16.0	14.9	15.1
ELTEMP	4.2	17.1	16.3	13.4
SYNCH	3.6	16.4	14.5	15.2

temperature T_e , while SYNCH is dominated by the post-acceleration synchrotron component.

Fitting data set 2 with similar parameter values (relating to the energy budget and assumed geometry) as data set 1 yields very poor statistics (best $\chi^2_{\text{red}} \sim 30$). Trying to model the steep X-ray spectrum, mainly employing the exponential decay of the multicolour disc,

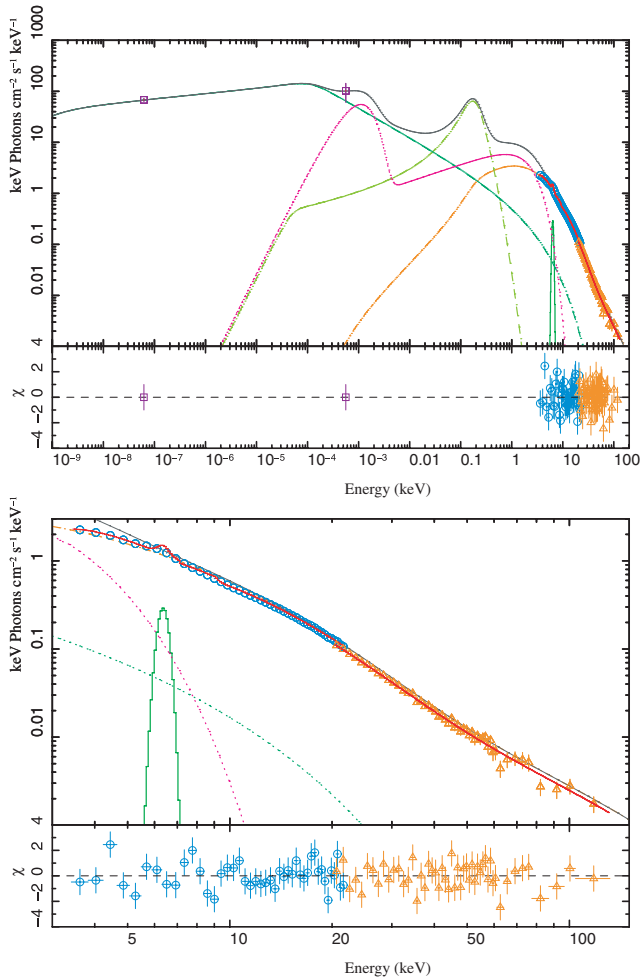


Figure 10. Multiwavelength (top) and X-ray band only (bottom) bestfitting result ($\chi_{\text{red}}^2 \sim 1.0$) spectrum, for the 2005 data set, using a reduced low electron temperature $T_e \sim 4 \times 10^9$ K (cf. Table 3, *ELTEMP* column).

fails, because a higher disc contribution offers more (soft) seed photons. These photons are up-scattered and create a Compton tail in the hardest part of the spectrum where they overestimate the observed flux.

We therefore searched the parameter space for any other solution that reduces the flux of Comptonized high-energy photons by reducing the electron temperature T_e . A lower temperature electron distribution would on average not up-scatter the disc seed photons to equally high energy. We find that if we allow T_e to evolve freely, we end up with a very good fit ($\chi_{\text{red}}^2 \sim 0.7$); however, the final temperature is rather low. At $\sim 4 \times 10^9$ K the bulk of the electrons would be subrelativistic. The use of a relativistic Maxwell–Jüttner distribution, as done in the MNW05 model, would no longer be fully justified, as the majority of the particles in the thermal distribution would have $\gamma = 1$. However, this approach effects a very peaked and steep pre-shock synchrotron component. This distribution of seed jet-base photons allows for a Comptonized photon distribution that is steep enough to fit the X-ray data up to 50 keV. Above 50 keV the Comptonized disc photons harden the model spectrum just enough to fit the entire range of HEXTE data.

An alternative possibility for fitting data set 2 – with an increased electron temperature – is found when we increase the ratio of synchrotron to inverse Compton emission. With synchrotron dominant below ~ 30 keV (see Fig. 11 and Table 3, *SYNCH* column) and

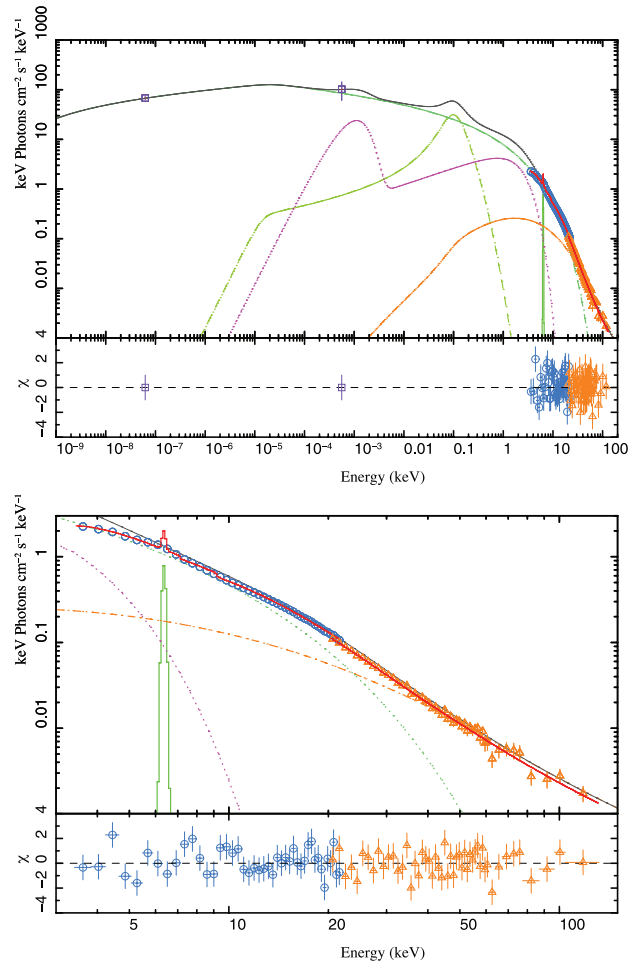


Figure 11. Multiwavelength (top) and X-ray band only (bottom) bestfitting result ($\chi_{\text{red}}^2 \sim 1.15$) spectrum, for the 2005 data set, using the synchrotron cut-off to fit the X-ray (cf. Table 3, *SYNCH* column).

cut-off at about 1 keV, the subsequent exponential decay can approximate the X-ray features rather well, when combined with an accretion disc peaking at the same energy (Fig. 11). In general we feel that, given the unknowns in the exact shape of the particle distribution around the cut-off, it is undesirable to rely on this in general during the fits. However, it is worth noting that it provides a very good description of the data ($\chi_{\text{red}}^2 \sim 0.7$). Fitting with the synchrotron cut-off requires a very hard synchrotron spectrum ($\Gamma \sim 1.2$). Normally such a hard spectral index would be expected only in ultrarelativistic sources (e.g. Heavens & Drury 1988). As for the SMEDGE2 fit, the relatively shallow spectrum could, however, again be (partly) reconciled with the canonical values for p , considering the effect of cooling on the spectrum.

4.3 Stellar companion spectrum

While the predominant temperature of a K2 star is 4455 K, the data set 1 fits show a systemic discrepancy that could be resolved increasing the blackbody temperature (and normalization). While the temperature of 4455 K is the predominant value for a solitary class 2 star of this type, clearly this is not the case for the companion of GRS 1915+105.

Although the physical properties of stars under these conditions are still largely undetermined, Kaper (2001) resolved discrepancies

in the effective temperatures of donor stars in high-mass X-ray binaries, of 10–25 per cent higher than expected from their spectral classification. Increasing the temperature of our blackbody by 25 per cent to 5500 K results in an insignificant improvement in fit by $\Delta\chi_{\text{red}}^2 = 0.03$.

Letting the temperature and normalization of the blackbody in our best-fitting result `SMEDGE` free to vary improves the χ_{red}^2 to $81/165 = 0.5$, but yields an extremely high blackbody temperature of $1.33^{+0.14}_{-0.04} \times 10^5$ K. Such an exceedingly high temperature indicates that other IR contributions than photospheric emission from the secondary are likely. Chaty et al. (1996) already concluded the same from the rapid variations and spectral shape they observed in this band. In particular, irradiation of the companion star and/or the disc for a source as bright as GRS 1915+105 should be quite significant, but the former is not accounted for in detail in our modelling, while the latter is not accounted for at all. Using an irradiated disc+jet model, Maitra et al. (2009) obtained disc temperatures for XTE J1118+480 in the order of a few tens of thousands kelvin, in agreement with, e.g. Hynes et al. (2006). Our obtained temperature of $\sim 1.3 \times 10^5$ K seems rather high; however, XTE J1118+480 accretes at rates $\lesssim 10$ per cent L_{Edd} , while for GRS 1915+105 this is $\sim L_{\text{Edd}}$. Other possibilities for IR contributions include optically thick free–free emission (although usually not observed at such high energies), or optically thin free–free radiation from an X-ray-driven accretion disc wind (Castro-Tirado, Geballe & Lund 1996; Fuchs, Mirabel & Claret 2003a).

5 DISCUSSION

Clearly, and perhaps surprisingly, there are large differences between data sets 1 and 2, both in the χ state of GRS 1915+105. While data set 1 can be fit fairly well by the same model as for BHBs, data set 2 is marginal, thus they do not seem to represent a standard class of spectral behaviour. Interestingly, Rau & Greiner (2003) also find significant variety between the individual χ states they observed in over 4 yr. While the classification done by Belloni et al. (2000) is based on light curves and colour–colour diagrams, the subindices 1–4 do not refer to a phenomenological classification scheme, but only denote their temporal sequence. Hence there remains the possibility that the χ state still encompasses multiple physical regimes that we may be probing here via spectral fitting.

Alternatively, data set 2 could be in some kind of transitional state, despite being classified as a typical χ state. In GRS 1915+105 complete state changes can happen on very short time-scales in comparison to the canonical BHs (seconds). Such rapid changes generally occur only between states A and B, however. While state C episodes can also last for short periods of < 100 s, the current data sets involve only the longer (a day or more) intervals. As indicated by the radio and NIR light curves, it is clearly possible that during the data set 2 observations GRS 1915+105 was in a transitional state and therefore the model, which assumes a steady outflow, is no longer applicable. Either way, both of the statistically convincing data set 2 fits (`SYNCH` and `ELTEMP`) have other problems in their physical interpretation, as discussed above, and it is possible that the model simply cannot apply to observations at such high luminosities (see Fig. 1).

For all of the fits presented, two parameters consistently stand out by nature of their larger values when compared to applications of the MNW05 model to BHBs: the location of initial particle acceleration in the jets, z_{acc} , and the energy partition parameter k . As mentioned before, we typically find z_{acc} 1–2 orders of magnitude

closer in towards the base of the jets in fits of other BHBs in the HS. Similarly, while the canonical BHBs often display mild magnetic domination over the gas pressure, with $k \simeq 10$, we find that at least an order of magnitude increase is needed to fit GRS 1915+105 plateau states. Finally, the overall powers required (as indicated by the jet normalization parameter N_j ; see MNW05 for an explanation) are strikingly larger than the maximum observed in other BHBs. Canonical BHBs displaying these luminosity levels in L_{Edd} would long have shut down their jets, yet somehow GRS 1915+105 seems to be operating on a different energy scale.

These three parameters may well be related. Magnetic fields are by now known to play a major role in accelerating and collimating relativistic plasma outflows, and current simulations of jet formation favour rather high values of k (usually expressed as low values of the plasma β , denoting the ratio of the magnetic to gas pressure; e.g. McKinney 2006; Komissarov et al. 2007; McKinney & Blandford 2009). It may be that k is positively correlated with the overall power input into the jets. Evidence for such a scaling has already been observed in individual fits to broad-band data of the LLAGN M81* over the course of a year-long campaign (see, e.g. Markoff et al. 2008, fig 22). The overall magnetic field strength and configuration will certainly influence the formation of particle acceleration structures; however, the dependence on total power and other parameters has not yet been thoroughly explored. A higher level of magnetic domination can also account for why the fits favour an electron temperature T_e that is a factor of 2 or more lower than the the bottom of the range ($\sim 2\text{--}7 \times 10^{10}$ K) found for the canonical microquasars. A stronger magnetic field relative to the radiating plasma at the base of the jets in our model is synonymous with the same being true at the inner edge of the accretion flow, as we assume they are directly related. A relatively stronger magnetic field would result in relatively more lepton cooling in the inner regions, and consequently a lower equilibrium temperature.

In contrast, the geometry of both the base of the jets and the cool accretion disc parameters preferred in the fits is entirely consistent with the range found in the canonical BHBs. The radius of the base of the jets is $3\text{--}20 r_g$ exactly as seen in fits of both BHBs as well as LLAGN. Similarly, we obtain best-fitting values for the inner cool accretion disc radius $r_{\text{in}} \sim 2.5\text{--}4.7 r_g$, which is consistent with such a high accretion rate, as well as a spinning black hole as suggested by McClintock et al. (2006). What is not consistent, and differs compared to other BHB fits, is that the jet-base radius in most fits is larger (sometimes only marginally) than r_{in} . Since in our model the jets should be launched by the inner, hot accretion flow, this is not internally self-consistent and by such criteria, only fits `SMEDGE2` and `ELTEMP` would survive. As the MNW05 model does not yet self-consistently solve the jet-launching physics from a corona, which is still an unsolved problem, we have not made this a hard constraint.

Although in most BHBs such a small r_{in} would be indicative of a soft state, this is not true for GRS 1915+105. Due to the high accretion rate, a geometry where the accretion disc reaches the innermost stable orbit is almost expected. The fact that the `6KPC` fit has an inner radius of less than $1 r_g$ is most certainly due to the oversimplifications mentioned above and similar inner radii were also obtained for the canonical BHs (see, e.g. MNW05). In fact, such small radii appear to be a common occurrence, also using other models: analysing 4 yr of χ state observations Rau & Greiner (2003) obtained inner radii of far less than $1 r_g$, from the normalization of the disc contribution using the `DISKBB` model. Although this model is known to underestimate the inner disc radius by a factor of 1.7–3, due to Doppler blurring and gravitational redshift,

the obtained radii are still unrealistically low. The disc temperatures of 1–4 keV they find are higher than ours (0.7–0.9 keV), but again the DISKBB model is known to produce a factor of 1.7 overestimates (Lee et al. 2002). Comparing the two plateau states to each other, the required disc contribution is much higher in data set 2. For data set 1, however, disc normalizations are high but comparable to those for the canonical BHBs, suggesting that, as is true for the HS, the classification of individual plateau states should not be based on the luminosity.

In agreement with the findings of many other authors (e.g. Rau & Greiner 2003; Sobolewska & Życki 2003) who have studied the χ state, we find that the inverse Compton component is always dominant over the direct accretion disc contribution in the X-ray regime for our data sets, although in our case the Comptonization is mainly due to SSC rather than purely from thermal accretion disc seed photons. Only in one data set 2 fit (SYNCH) are the X-rays not dominated by the Comptonization, but the validity of this fit may be questionable on other grounds as discussed above.

As it was brought up as a potential issue by Maitra et al. (2009) and Malzac, Belmont & Fabian (2009), for high luminosities conditions at the base of the jet may comprise high enough photon densities that pair production can become important. As these processes are not yet implemented in the MNW05 model, we check the pair production and annihilation rates (\dot{n}_{pp} and \dot{n}_{pa} , respectively) at the base of the jets using the methods described in Maitra et al. (2009), and references therein. The results are shown Table 4. If the lepton number density n is not larger than $\dot{n}_{pp}r_0/c$ and $\dot{n}_{pa}r_0/c$, where r_0/c is roughly the *residence time* for the leptons in the jet-base region, we need $\dot{n}_{pp} < \dot{n}_{pa}$ to be able to neglect pair production.

Although our $T_e \lesssim 10^{10}$ is a factor of 5–6 lower than the limit deemed problematic for GX339-4, the extreme luminosity of GRS 1915+105 means that pair production could potentially be an issue for some of our fits. The source of potential pair production is a high-energy tail above ~ 0.5 MeV, due to the Comptonization of thermal accretion disc photons. The amount of flux in this tail is directly dependent on the normalization and temperature of the accretion disc component, which itself is mainly constrained by the value of N_H and the predicted flux in the tail region. Higher values of N_H result in higher accretion disc fluxes to compensate for the increased absorption in the soft X-ray band.

While we fixed the value for N_H in our X-ray fits to $4.7 \times 10^{22} \text{ cm}^{-2}$, an increasing number of works are concluding that the column density is actually variable, ranging in values from $N_H \sim 2 - 16 \times 10^{22} \text{ cm}^{-2}$ and potentially linked with an intrinsic warm absorber at the highest values (Belloni et al. 2000; Klein-Wolt et al. 2002; Lee et al. 2002; Yadav 2006). Although generally the column density derived from X-ray measurements is higher than those obtained using IR methods, we find that the highest values of the N_H range are not consistent with our model. Values $\gtrsim 7$ cause too great a decrease below 3 keV, resulting in too much flux in the high-energy tail, due to enhanced disc Comptonization. We chose the above more ‘average’ value for N_H , in order to be consistent with prior X-ray fits of the various χ substates (e.g. $2 \times 10^{22} \text{ cm}^{-2}$; Belloni et al. 1997a) and the assumptions of Chaty et al. (1996). For data set 2 the above value is likely too high. Letting N_H free to vary (without correcting the NIR dereddening accordingly), while maintaining a higher electron temperature of $\sim 10^{10}$ K settles on the lower bound allowed of $2 \times 10^{22} \text{ cm}^{-2}$, with a significant improvement in χ^2_{red} (from ~ 30 to ~ 25), mainly due to the resulting reduction in the Comptonized high-energy tail. Therefore, our results are highly dependent on the value of N_H , and that this value is likely different for the two data sets, although for the reasons described above we

have chosen to use a single value. Similarly, the uncertainty in the exact value means that too much pair production can be avoided in particular by lower values of N_H . Lower values are favoured if we allow N_H to vary, and interestingly this is consistent with the conclusion by Neilsen & Lee (2009) that the presence of an absorbing disc wind at high accretion rates should be anticorrelated with the presence of jets.

6 CONCLUSIONS

Despite the fact that the MNW05 model was originally intended for application to hard states in canonical BHBs only, it appears to well approximate the plateau state in GRS 1915+105. However, it does not produce convincing results in every instance. While some of the parameter values obtained are quite extreme, the results for the data set 1 appear credible and consistent with what we have found in canonical BHBs. Data set 2, however, presents more difficulties, and a more solid determination of the distance and absorption column would go far to help us understand the difference between these two plateau states.

Clearly, this work confirms that GRS 1915+105 is in a much more extreme range of parameter space for an outflow-dominated model, requiring near- or super-Eddington accretion rates, maximal jet powers and high levels of magnetic domination. Although our results confirm previously noted plateau state issues, such as the need for a variable N_H , our model for the first time incorporates the entire broad-band and has allowed the comparison between the jet producing plateau and hard states. While the baseline geometry seems similar, the plateau states of GRS 1915+105 are not low-luminosity as with HS BHBs, and settle on a range where the acceleration of particles occurs much further out in the jets, which can be 2 orders of magnitude further out of equipartition in the direction of magnetic domination. While these two effects may be linked, the model explored here cannot self-consistently address this, but in another work we are exploring the links between physical parameters and the location of particle acceleration fronts (Polko et al., in preparation). A slightly lower electron temperature is also found compared to other BHBs, which can be interpreted in the context of the higher cooling rates found at GRS 1915+105’s extreme luminosity.

The main consequence of these differences is that the synchrotron component from the outer jets no longer dominates the soft X-ray band, although a non-negligible X-ray synchrotron flux of ~ 10 per cent the inverse Compton flux below ~ 50 keV seems required for the statistically favoured fits. In comparison, the MNW05 model applied to canonical BHBs favours synchrotron emission dominating the flux at least up to 10 keV. Interestingly, our results are thus qualitatively similar to the results found from the blazar sequence (e.g. Ghisellini et al. 1998), where higher powers correspond to a decrease in the frequency range where synchrotron power peaks. It is clear that time-dependent effects such as cooling breaks demand further exploration, and we are currently working to implement them into more complex models.

The remarkable differences between the two individual plateau state observations does raise questions about whether the χ substates are distinct enough to classify all plateau characteristics. While both data sets explored here bear all the characteristics of the plateau state, the fits with a single model show more variations in free parameters than found even between different sources in the HS of canonical BHBs. Thus the current classification scheme based solely on X-ray colours and timing properties may need to be expanded based on broad-band attributes.

Our results support a conclusion that, although expressing quite different properties than the HS in canonical BHBs, GRS 1915+105 plateau states can still be described by the same broad-band model with a steady outflow tied in power to the accretion inflow. However, the BHB model is clearly forced into very extreme ranges, which themselves provide some new clues about the relationship between accretion rate, jet production and particle acceleration.

Although GRS 1915+105 is one of the most extensively studied BHBs over the last decades since its discovery, we are far from understanding this source. At some point in the future (somewhere this century, assuming the source went into outburst when it was first discovered; Deegan, Combet & Wynn 2009) GRS 1915+105 will invariably retreat into quiescence, and should finally yield better insight into the connection between its current accretion properties and those at sub-Eddington rates.

ACKNOWLEDGMENTS

The Green Bank Interferometer is a facility of the National Science Foundation operated by the NRAO in support of NASA High Energy Astrophysics programmes.

SM and DM acknowledge support from a Netherlands Organization for Scientific Research (NWO) Vidi and VC Fellowship, respectively.

The research leading to these results has received funding from the European Community's Seventh Framework Programme (FP7/2007-2013) under grant agreement number ITN 215212 'Black Hole Universe'.

AJCT acknowledges support from the Spanish Ministry program AYA 2009-14000-C03-01.

REFERENCES

- Alonso A., Arribas S., Martínez-Roger C., 1999, *A&AS*, 140, 261
- Arnaud K. A., 1996, in Jacoby G. H., Barnes J., eds, *Astronomical Society of the Pacific Conference Series*, Vol. 101, *Astronomical Data Analysis Software and Systems V*, p. 17
- Baars J. W. M., Genzel R., Pauliny-Toth I. I. K., Witzel A., 1977, *A&A*, 61, 99
- Belloni T., Mendez M., King A. R., van der Klis M., van Paradijs J., 1997a, *ApJ*, 488, L109
- Belloni T., Mendez M., King A. R., van der Klis M., van Paradijs J., 1997b, *ApJ*, 479, L145
- Belloni T., Klein-Wolt M., Méndez M., van der Klis M., van Paradijs J., 2000, *A&A*, 355, 271
- Cardelli J. A., Clayton G. C., Mathis J. S., 1989, *ApJ*, 345, 245
- Castro-Tirado A. J., Brandt S., Lund N., 1992, *IAU Circ.*, 5590, 2
- Castro-Tirado A. J., Brandt S., Lund N., Lapshov I., Sunyaev R. A., Shlyapnikov A. A., Guziy S., Pavlenko E. P., 1994, *ApJS*, 92, 469
- Castro-Tirado A. J., Geballe T. R., Lund N., 1996, *ApJ*, 461, L99
- Chapuis C., Corbel S., 2004, *A&A*, 414, 659
- Chaty S., 1998, PhD thesis, Service d'Astrophysique, CE Saclay, France
- Chaty S., Mirabel I. F., Duc P. A., Wink J. E., Rodríguez L. F., 1996, *A&A*, 310, 825
- Chiar J. E., Tielens A. G. G. M., 2006, *ApJ*, 637, 774
- Corbel S., 2000, in Strohmayer T. E., ed., *Rossi 2000: Astrophysics with the Rossi X-ray Timing Explorer*, Natl. Aeronautical Space Admin., Greenbelt, MD
- Corbel S., Fender R. P., Tzioumis A. K., Nowak M., McIntyre V., Durouchoux P., Sood R., 2000, *A&A*, 359, 251
- Corbel S., Nowak M. A., Fender R. P., Tzioumis A. K., Markoff S., 2003, *A&A*, 400, 1007
- Coriat M., Corbel S., Buxton M. M., Baylin C. D., 2009, in Rodríguez J., Ferrando P., eds, *AIP Conf. Ser. Vol. 1126, Symbol-X: Focusing on the Hard X-Ray Universe*. Am. Inst. Phys., New York, p. 207
- Deegan P., Combet C., Wynn G. A., 2009, *MNRAS*, 1549
- Dhawan V., Mirabel I. F., Rodríguez L. F., 2000, *ApJ*, 543, 373
- Ebisawa K., 1991, PhD thesis, Univ. Tokyo; ISAS Research Note No. 483, (1991)
- Falcke H., Körding E., Markoff S., 2004, *A&A*, 414, 895
- Falcke H., Markoff S., Bower G. C., 2009, *A&A*, 496, 77
- Feldt M., Stecklum B., Henning T., Hayward T. L., Lehmann T., Klein R., 1998, *A&A*, 339, 759
- Fender R., Belloni T., 2004, *ARA&A*, 42, 317
- Fender R. P., Garrington S. T., McKay D. J., Muxlow T. W. B., Pooley G. G., Spencer R. E., Stirling A. M., Waltman E. B., 1999, *MNRAS*, 304, 865
- Foster R. S., Waltman E. B., Tavani M., Harmon B. A., Zhang S. N., Paciasas W. S., Ghigo F. D., 1996, *ApJ*, 467, L81+
- Fuchs Y., Mirabel I. F., Claret A., 2003a, *A&A*, 404, 1011
- Fuchs Y. et al., 2003b, *A&A*, 409, L35
- Gallo E., Fender R. P., Pooley G. G., 2003, *MNRAS*, 344, 60
- Gallo E., Migliari S., Markoff S., Tomsick J. A., Bailyn C. D., Berta S., Fender R., Miller-Jones J. C. A., 2007, *ApJ*, 670, 600
- Ghisellini G., Celotti A., Fossati G., Maraschi L., Comastri A., 1998, *MNRAS*, 301, 451
- Greiner J., Cuby J. G., McCaughrean M. J., 2001a, *Nat*, 414, 522
- Greiner J., McCaughrean M. J., Cuby J. G., Castro-Tirado A. J., Mennickent R. E., 2001b, *Ap&SS*, 276, 31
- Hannikainen D. C. et al., 2005, *A&A*, 435, 995
- Harlaftis E. T., Greiner J., 2004, *A&A*, 414, L13
- Heavens A. F., Drury L. O., 1988, *MNRAS*, 235, 997
- Homan J., Belloni T., 2005, *Ap&SS*, 300, 107
- Houck J. C., Denicola L. A., 2000, in Manset N., Veillet C., Crabtree D., eds, *ASP Conf. Ser. Vol. 216, Astronomical Data Analysis Software and Systems IX*. Astron. Soc. Pac., San Francisco, p. 591
- Hynes R. I. et al., 2006, *ApJ*, 651, 401
- Jahoda K., Markwardt C. B., Radeva Y., Rots A. H., Stark M. J., Swank J. H., Strohmayer T. E., Zhang W., 2006, *ApJS*, 163, 401
- Kaper L., 2001, in Vanbeveren D., ed., *Astrophys. Space Sci. Library*, Vol. 264, *The Influence of Binaries on Stellar Population Studies*. Springer-Verlag, Berlin, p. 125
- Kardashev N. S., 1962, *SvA*, 6, 317
- Klein-Wolt M., Fender R. P., Pooley G. G., Belloni T., Migliari S., Morgan E. H., van der Klis M., 2002, *MNRAS*, 331, 745
- Komissarov S. S., Barkov M. V., Vlahakis N., Königl A., 2007, *MNRAS*, 380, 51
- Leahy D. A., Darbro W., Elsner R. F., Weisskopf M. C., Kahn S., Sutherland P. G., Grindlay J. E., 1983, *ApJ*, 266, 160
- Lee J. C., Reynolds C. S., Remillard R., Schulz N. S., Blackman E. G., Fabian A. C., 2002, *ApJ*, 567, 1102
- Magdziarz P., Zdziarski A. A., 1995, *MNRAS*, 273, 837
- Maitra D., Markoff S., Brocksopp C., Noble M., Nowak M., Wilms J., 2009, *MNRAS*, 398, 1638
- Malzac J., Belmont R., Fabian A. C., 2009, *MNRAS*, 1453
- Markoff S. et al., 2008, *ApJ*, 681, 905
- Markoff S., Nowak M. A., Wilms J., 2005, *ApJ*, 635, 1203
- McClintock J. E., Remillard R. A., 2003, preprint (astro-ph/0306213)
- McClintock J. E., Shafee R., Narayan R., Remillard R. A., Davis S. W., Li L.-X., 2006, *ApJ*, 652, 518
- McKinney J. C., 2006, *MNRAS*, 368, 1561
- McKinney J. C., Blandford R. D., 2009, *MNRAS*, 394, L126
- Merloni A., Heinz S., di Matteo T., 2003, *MNRAS*, 345, 1057
- Migliari S. et al., 2007, *ApJ*, 670, 610
- Mirabel I. F., Rodríguez L. F., 1994, *Nat*, 371, 46
- Mirabel I. F., Rodríguez L. F., 1998, *Nat*, 392, 673
- Muno M. P., Remillard R. A., Morgan E. H., Waltman E. B., Dhawan V., Hjellming R. M., Pooley G., 2001, *ApJ*, 556, 515
- Naik S., Rao A. R., 2000, *A&A*, 362, 691

- Neil E. T., Bailyn C. D., Cobb B. E., 2007, *ApJ*, 657, 409
Neilsen J., Lee J. C., 2009, *Nat*, 458, 481
Pooley G. G., Fender R. P., 1997, *MNRAS*, 292, 925
Rao A. R., Naik S., Vadawale S. V., Chakrabarti S. K., 2000, *A&A*, 360, L25
Rau A., Greiner J., 2003, *A&A*, 397, 711
Reig P., Belloni T., van der Klis M., 2003, *A&A*, 412, 229
Remillard R. A., McClintock J. E., 2006, *ARA&A*, 44, 49
Rodriguez J., Durouchoux P., Mirabel I. F., Ueda Y., Tagger M., Yamaoka K., 2002, *A&A*, 386, 271
Rodriguez J. et al., 2008a, *ApJ*, 675, 1436
Rodriguez J. et al., 2008b, *ApJ*, 675, 1449
Rodriguez L. F., Gerard E., Mirabel I. F., Gomez Y., Velazquez A., 1995, *ApJS*, 101, 173
Rothschild R. E. et al., 1998, *ApJ*, 496, 538
Russell D. M., Fender R. P., Hynes R. I., Brocksopp C., Homan J., Jonker P. G., Buxton M. M., 2006, *MNRAS*, 371, 1334
Russell D. M., Maitra D., Dunn R. J. H., Markoff S., 2010, *MNRAS*, 405, 1759
Shakura N. I., Sunyaev R. A., 1973, *A&A*, 24, 337
Sobolewska M. A., Życki P. T., 2003, *A&A*, 400, 553
Tagger M., Varnière P., Rodriguez J., Pellat R., 2004, *ApJ*, 607, 410
Trudolyubov S. P., 2001, *ApJ*, 558, 276
Ueda Y. et al., 2002, *ApJ*, 571, 918
Yadav J. S., 2006, *ApJ*, 646, 385

This paper has been typeset from a $\text{T}_{\text{E}}\text{X}/\text{L}^{\text{A}}\text{T}_{\text{E}}\text{X}$ file prepared by the author.